

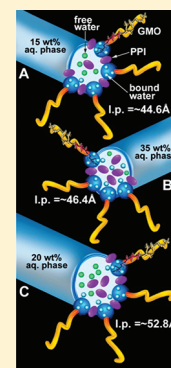
Structural Behavior and Interactions of Dendrimer within Lyotropic Liquid Crystals, Monitored by EPR Spectroscopy and Rheology

Liron Bitan-Cherbakovsky,[†] Dima Libster,^{*,†} Maria Francesca Ottaviani,[‡] Abraham Aserin,[†] and Nissim Garti^{*,†}

[†]The Ratner Chair of Chemistry, Casali Institute of Applied Chemistry, The Institute of Chemistry, The Hebrew University of Jerusalem, Edmond J. Safra Campus, Givat Ram, Jerusalem 91904, Israel

[‡]Department of Earth, Life and Environment Sciences, University of Urbino, Località Crocicchia, Urbino 61029, Italy

ABSTRACT: Micro- and macrostructural behaviors of three different lyotropic liquid crystals (LLCs) loaded with a dendrimer, namely second generation poly(propylene imine) (PPI-G2), were studied by means of rheology and electron paramagnetic resonance (EPR). The three mesophases were L_w , Q^{224} , and H_{II} composed of glycerol monooleate (GMO) and water–PPI-G2 solution (and D- α -tocopherol (vitamin E) in the case of H_{II}). We characterized the impact of PPI-G2 interactions with the components of the host mesophases on their structural characteristics on different length scales. The incorporation of PPI-G2 within the L_w and H_{II} systems induced the formation of more elastic hexagonal systems with a “solidlike” behavior, while in the Q^{224} system a different trend with a “liquidlike” behavior was observed. As a result, the dendrimer induced a remarkable change in both the structural and viscoelastic properties of the systems. Hence, the microenvironment in the interface region within the systems was monitored by computer-aided EPR using 5-doxylstearic acid (5-DSEA) as a pH-dependent probe. The microviscosity (τ) and order (S) of systems were found to be sensitive to the PPI-G2 presence: when PPI-G2 concentration increased, τ and S increased in both the L_w and Q^{224} systems. In the H_{II} systems two trends were observed, reflecting a decrease in τ and S up to 10 wt % PPI-G2 and subsequently their increase at higher dendrimer concentrations. It was assessed that PPI-G2 interacted strongly with the GMO hydroxyl groups in the L_w phase, with the water molecules in the Q^{224} systems. In the H_{II} mesophase strong interactions with both the water and GMO hydroxyl molecules were detected.



■ INTRODUCTION

Dendrimers, globular macromolecules with a unique well-defined “treelike” structure, are versatile candidates as vehicles for drugs or as scaffolds, mainly in cancer therapy and in the nanomedicine field.^{1–5} Dendrimers are characterized with a narrow polydispersity and nanometer size range that enable an easier passage through biological barriers.^{6,7} Their particular architecture consists of three parts from the interior to the surface: (i) a central core with a single atom or an atomic group having at least two identical chemical functions; (ii) repeated units that spread out from the central core, with at least one branch junction and organized in a geometrical progression that results in a series of radially concentric layers called generations; and (iii) several functional groups, located on the surface of the macromolecule, which determine the physical properties of the dendrimer.^{5,8–10} Due to the presence of multiple terminal groups on the exterior of the dendrimer, they provide an excellent platform for the attachment of drugs and cell-specific targeting groups. Dendrimers can also encapsulate hydrophobic drugs inside the nonpolar interior cavities present around the focal core of the dendrimer by a host–guest interaction.^{3,10–13} Another unique property of dendrimers is their ability to serve as therapeutic agents by themselves by virtue of their activities against prion and Alzheimer’s diseases,^{14,15} HIV,¹⁶ cancer, and other diseases.¹⁷

However, in comparison to colloidal carriers, it appears that dendrimers suffer from relatively low encapsulation capacity of

various drugs and their potential capability to sustain delivery of the encapsulated drugs is much lower. In this regard, in order to enhance the performance of dendrimers as delivery agents, in our previous work¹ we demonstrated for the first time a complex prospective drug delivery system, based on a dendrimer solubilized in the aqueous domains of lyotropic liquid crystals (LLCs) based on glycerol monooleate.

LLCs are promising candidates as alternative delivery vehicles for a wide range of molecules, such as both hydrophilic and hydrophobic drugs, nutraceuticals, and food additives. LLCs are formed by polar lipids and certain surfactants mixing with water.^{18–22} Recently, LLCs based on glycerol monooleate were extensively explored and shown to form several typical mesophases. The most significant inverse water-in-oil structures are the lamellar, cubic, and reverse hexagonal. These types of LLCs have been shown to provide improved solubility of drugs and bioactive molecules and sustained release of guest molecules with a range of physicochemical properties²³ and thermodynamic stability.^{20,24–29}

Owing to these properties, these mesophases can be specifically used to solubilize dendrimers and enhance their delivery as therapeutic agents for oral and transdermal release. As published,¹ a second generation (G2) of poly(propylene)

Received: December 13, 2011

Revised: February 5, 2012

Published: February 6, 2012

imine dendrimer (PPI) was solubilized into lamellar, diamond reverse cubic, and reverse columnar hexagonal LLCs composed of GMO (glycerol monooleate) and water (and D- α -tocopherol in the H_{II} system).

Consequently, $L_\alpha \rightarrow H_{II}$ and $Q^{224} \rightarrow H_{II}$ structural shifts were detected (at 20 and 10 wt % PPI-G2 content for L_α and Q^{224} , respectively), probably induced by the dehydration of GMO headgroups and subsequent increase of the lipid's critical packing parameter (CPP). In the case of direct incorporation of PPI-G2 into H_{II} mesophase, no structural transitions occurred. Hence, three types of hexagonal structures containing the same weight fraction of PPI-G2 in the aqueous phase, but differing in aqueous phase content, dendrimer localization, and lattice parameters, were accepted. In the current work, we acquired a deeper insight into the structural dissimilarities of the three hexagonal structures obtained via different precursors (L_α , Q^{224} , and H_{II} mesophases). Macroscopic behavior of these systems was assessed by rheological measurements, which have already been shown to distinguish between closely related liquid crystalline mesophases due to their different viscoelastic characteristics. Furthermore, rheological measurements correlated the macroscopic features of the systems with alterations on the molecular level, performed by electron paramagnetic resonance (EPR) spectroscopy. We have already demonstrated that different microenvironments within the H_{II} mesophase can be monitored by a computer-aided electron paramagnetic resonance (EPR) analysis using 5-doxylstearic acid (5-DSEA) as a pH-dependent probe.^{30–32} EPR also provides information about the unfolding/denaturation of insulin within the H_{II} mesophase channel at high temperatures.³⁰ Comprehensive understanding of the structural properties of the LLC/dendrimer complexes is imperative for rational and successful tailoring of these potential delivery vehicles. Characterization of the different levels of organization of these special materials and characterization of the detailed relationships and possible correlations between them are the major aims of this study.

■ EXPERIMENTAL SECTION

Monoolein (GMO), distilled glycerol monooleate that consists of 97.1 wt % monoglycerides, 2.5 wt % diglycerides, and 0.4 wt % free glycerol (acid value 1.2, iodine value 68.0, melting point 37.5 °C), was purchased from Riken (Tokyo, Japan). D- α -Tocopherol, vitamin E 5-96 (VE; containing 1430 international units of vitamin E), was obtained from ADM (Decatur, IL, USA). PPI (second generation) (>95% purity) was obtained from SyMO-Chem (The Netherlands). The spin probe 5-doxylstearic acid [2-(3-carboxypropyl)-4,4-dimethyl-2-tridecyl-3-oxazolidinyloxy], free radical, was purchased from Sigma-Aldrich (St. Louis, MO, USA). The spin probe was used as received. Hydrochloric acid (37%) was purchased from Sigma-Aldrich (St. Louis, MO, USA). Water was double distilled. All ingredients were used without further purification.

Sample Preparation. The GMO-based LLC samples were formed by adding the dendrimer aqueous phase (solution of PPI-G2 in distilled water at pH ~8.6–8.7, which formed by HCl (37% concentration) titration) to GMO in 15/85 and 35/65 ratios for the L_α and Q^{224} mesophases, respectively, and to GMO/VE (90/10 ratio) in an 80/20 ratio for the H_{II} mesophase. The aqueous phase content in each mesophase was kept constant (15, 35, and 20 wt % for L_α , Q^{224} , and H_{II} , respectively), while the PPI-G2 content in the aqueous phase was 0–30 wt %. After addition of the aqueous phase to GMO and to the GMO/VE mixture, the sample was heated to ~70

°C in sealed tubes under nitrogen (to avoid oxidation of the GMO) for ca. 15 min. The samples were stirred and cooled to 25 °C. It should be noted that as a result of PPI-G2 solubilization the concentrations of the water were decreased, keeping the weight ratio of GMO/D- α -tocopherol (9:1) and GMO with aqueous phase constant.

Rheological Measurements. Rheological measurements were performed using a Rheoscope 1 rheometer (Thermo-Haake, Karlsruhe, Germany). A cone–plate sensor was used with a diameter of 35 mm, cone angle of 1°, and a gap of 0.024 mm. The linear viscoelastic range (LVR) of a material was determined before the oscillatory measurements were carried out. The storage and loss moduli were plotted as a function of stress at frequency $\omega = 1$ Hz, at 25 °C (data not shown). The shear moduli were independent of stress up to a critical applied stress and generally were observed to fall off sharply beyond the values of 50, 227, and 600 Pa for L_α , Q^{224} , and H_{II} , respectively (it should be noted that, for 25 and 30 wt % PPI-G2 in the L_α phase, the value was 600 Pa). These results indicate that the samples of L_α , Q^{224} , and H_{II} possess linear viscoelastic properties up to about 50, 227, and 600 Pa, respectively. According to the determined LVR, the viscoelasticity measurements were generally performed at 25, 100, and 120 Pa for L_α , Q^{224} , and H_{II} , respectively (and 185 Pa for 25 and 30 wt % PPI-G2 in the L_α phase). Frequency-dependent rheological measurements were conducted in the range 0.01–100 rad/s. The viscoelasticity of the three mesophases was characterized in terms of the elasticity and the η^* , from which the complex viscosity G^* , the loss modulus G'' , and the longest relaxation time τ_{\max} could be evaluated. All of the tests, performed at 25 °C, were measured in triplicate and found to be reproducible.

Electron Paramagnetic Resonance (EPR) Measurements. *Insertion of the Probe.* The 5-DSEA probe was first dissolved in chloroform at a concentration of 2.5×10^{-3} M as a stock solution. An appropriate quantity of the probe solution was placed in tubes, and the solvent was then evaporated before preparation of the three mesophases within these tubes. A low concentration of 1×10^{-4} M probe in the examined LLC systems was used for all EPR studies. Such a low concentration has already been demonstrated to not perturb the nanostructures.

EPR Instrumentation and Method. EPR spectra were recorded at room temperature using a Bruker EMX spectrometer operating at the X band (9.5 GHz) using Pyrex capillary tubes (~1 mm inner diameter) as sample containers. The spectra were recorded 24 h after sample preparation. The EPR experiment setup includes a modulation amplitude of 1 G, microwave frequency of 9.42 GHz, center magnetic field of 3355.00 G, sweep width of 200.00 G, resolution of 1024 points, time constant of 0.32 ms, and conversion time of 10.24 ms, with a coherent acquisition of 49 scans per each EPR spectrum.

■ RESULTS AND DISCUSSION

In our previous paper¹ we demonstrated for the first time incorporation of a dendrimer into three lyotropic liquid crystalline mesophases. Consequently, $L_\alpha \rightarrow H_{II}$ and $Q^{224} \rightarrow H_{II}$ structural shifts were detected (at 20 and 10 wt % PPI-G2 content for L_α and Q^{224} , respectively), probably induced by the dehydration of GMO headgroups and subsequent increase of the lipid's critical packing parameter (CPP). In the case of direct incorporation of PPI-G2 into the H_{II} mesophase, no structural transitions occurred.¹

These phenomena were explained by interplay between two competing processes. The first is the dehydration of the monoolein headgroups, reducing their area. The second is strong intercalation of the macromolecules to the interfacial region, increasing the number of hydrogen bonds there.

Rheological Measurements. Rheological measurements were used to evaluate the impact of the dendrimer on the macroscopic mechanical properties of LLC systems and to correlate their mesophases with microscopic characteristics obtained by EPR and small-angle X-ray scattering (SAXS) analysis.

Frequency-dependent measurements were performed to establish the storage modulus $G'(\omega)$, loss modulus $G''(\omega)$, and complex viscosity η^* values of PPI-G2-loaded LLCs. As a result of PPI-G2 solubilization in the L_α mesophase, a reduction in the lattice parameter occurred (Table 1), accompanied by

Table 1. Lattice Parameter a ($\text{\AA} \pm 0.5 \text{\AA}$), Type of Mesophase, Gel Strength Parameter (S), and Strength of Intermolecular Interactions (m) of Three Different PPI-G2 Loaded and Unloaded Mesophases at pH 8.6^a

| aqueous phase (wt%) | PPI-G2 (wt %) | lattice parameter (\AA) | mesophase | S | m |
|---------------------|---------------|------------------------------------|-----------------------|---------|---------|
| 15 | 0 | 41.67 | L_α | 345 | -0.75 |
| | 5 | 40.67 | L_α | 86 959 | -0.8669 |
| | 10 | 39.32, 44.88 | L_α , H_{II} | | |
| | 15 | 38.8, 44.4 | L_α , H_{II} | | |
| | 20 | 44.13 | H_{II} | 49 941 | -0.7851 |
| | 25 | 44.66 | H_{II} | 89 538 | -0.8338 |
| | 30 | 44.88 | H_{II} | 105 058 | -0.8418 |
| 30 | 0 | 125 | Q^{224} | 89 732 | -0.9849 |
| | 5 | 117.5 | Q^{224} | 60 643 | -0.9474 |
| | 10 | 51.8 | H_{II} | 37 811 | -0.7608 |
| | 15 | 49.32 | H_{II} | 22 295 | -0.7532 |
| | 20 | 47.28 | H_{II} | 34 385 | -0.7406 |
| | 25 | 46.4 | H_{II} | 19 633 | -0.7429 |
| | 30 | 45.93 | H_{II} | 13 135 | -0.7469 |
| 20 | 0 | 54.5 | H_{II} | 67 085 | -0.7633 |
| | 5 | 55.3 | H_{II} | 38 775 | -0.8071 |
| | 10 | 56.7 | H_{II} | 47 731 | -0.8178 |
| | 15 | 55.3 | H_{II} | 39 774 | -0.7642 |
| | 20 | 54 | H_{II} | 38 078 | -0.7452 |
| | 25 | 52.8 | H_{II} | 32 097 | -0.699 |
| | 30 | 52.5 | H_{II} | 36 728 | -0.737 |

^aThe three mesophases are GMO + 15 wt % aqueous phase, GMO + 35 wt % aqueous phase, and GMO/VE (90/10) + 20 wt % aqueous phase. Note the italic font indicates the presence of a mixture of two mesophases.

the formation of the H_{II} mesophase, at PPI-G2 content of 5–15 wt %. The $L_\alpha \rightarrow H_{II}$ structural transition was completed upon addition of 20 wt % PPI-G2.

Figure 1a shows the mechanical moduli (G' and G'') as a function of frequency for the L_α phase at 25 °C and 15 wt % water content. In accordance with the literature,^{18,33} the L_α phase behaves as a plastic material, demonstrating relatively low values of both moduli ($<1000 \text{ Pa}$).¹⁸ While G' dominates over a low frequency spectrum, G'' increases smoothly until it reaches the values of the elastic moduli. According to the terminology used by Mezzenga et al.,¹⁸ this behavior was classified as transition to flow (at low frequencies, up to 1 rad/s) followed by a rubbery plateau ($\omega > 1 \text{ rad/s}$). Incorporation of PPI-G2 at

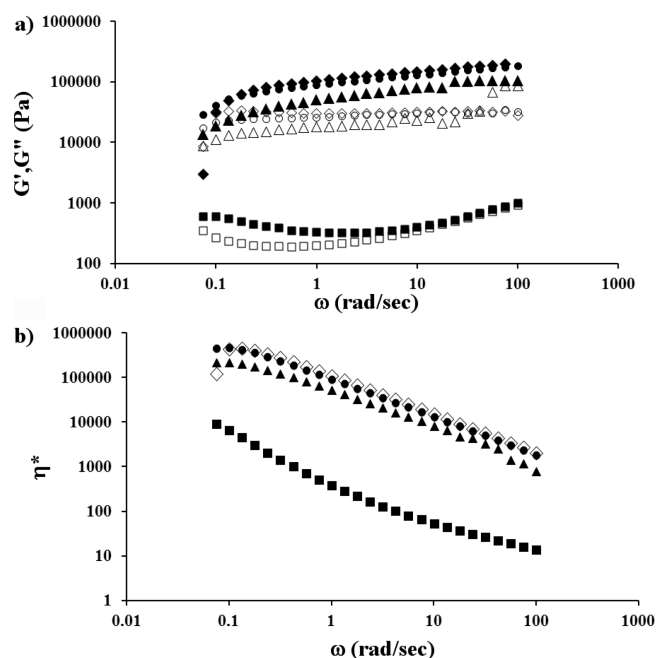


Figure 1. (a) Dynamic frequency sweep test for GMO (85 wt %) and aqueous phase (15 wt %) containing G' (■) and G'' (□), G' (▲) and G'' (△), G' (●) and G'' (○), and G' (◆) and G'' (◇) of 0, 20, 25, and 30 wt % PPI-G2 at 25 °C. (b) Complex viscosity (η^*) as a function of the applied oscillation frequency (ω) of GMO (85 wt %) and 15 wt % aqueous phase containing (■) 0, (▲) 20, (●) 25, and (◇) 30 wt % PPI-G2, all at 25 °C.

20–30 wt % from the aqueous phase, which induced the described transition to the H_{II} mesophases, was straightforwardly identified by tracking the evolvement of the mechanical moduli (Figure 1a). Both G' and G'' of the H_{II} mesophases were found to be 2 orders of magnitude higher than those of the empty L_α phase, implying more rigid samples. Increasing the PPI-G2 concentration caused higher values of G' , thereby inducing an increase in the elasticity of the samples. The elastic modulus remained higher than the viscous modulus (G'') in the whole examined frequency range, suggesting gel-like behavior and relaxation times longer than those reported for other H_{II} mesophases.^{33,34} Previously, a typical oscillatory sweep curve's behavior of the H_{II} system was reported in several publications.^{26,35,36} The dynamic moduli of the investigated H_{II} mesophases (13–22 wt % water content) were shown to comply with quasi-Maxwellian frequency dependence functions^{26,35,36} characterized by the longest relaxation time (τ_{\max}), calculated as the reciprocal frequency at the crossover point of the storage and loss moduli ($1/\omega$). Therefore, the solubilization of PPI-G2 changed the rheological behavior of GMO-based H_{II} mesophases. PPI-G2 induced formation of very rigid hexagonal structures, which did not obey quasi-Maxwellian frequency dependence, possessing low aqueous phase content (15 wt %), high curvature, and small lattice parameter (44 Å). Since the major rheological properties of the different phases depend primarily on the topology of the water–lipid interface,¹⁸ we can suggest that the presence of the PPI-G2 led to changes in the GMO–water interface during the transformation into more “solidlike” behavior.

Reinforcement of the observed trend was obtained by plotting the complex viscosity of these samples versus the oscillation frequency. As seen in Figure 1b, all samples possessed a shear thinning behavior typical of viscoelastic

materials. η^* is 10 000 Pa·s in the L_α phase and between 200 000 and 450 000 Pa·s (at $\omega = 0.1$ rad/s) in the H_{II} mesophases (as a function of PPI-G2 content), nicely capturing the $L_\alpha \rightarrow H_{II}$ structural shift.

The decrease of complex viscosity (η^*) with frequency tends to follow a power law in the entire frequency range (eq 1):

$$\eta^* = S\omega^m \quad (1)$$

where S is the gel strength parameter, which depends on the strength of intermolecular interactions, and m is the complex viscosity relaxation exponent (Figure 1b). Values of m close to zero indicate a liquidlike behavior, while values of m approaching -1 suggest a solidlike response of the system (Table 1). It was observed that incorporation of PPI-G2 induced more solidlike behavior of the mesophases, according to the lower S and m absolute values (Table 1). A significant increase in the S values from 345 in the case of empty L_α mesophase to 50 000–105 000 in the presence of 20–30 wt % PPI-G2 in the H_{II} structure was noticed, and higher m values (from -0.75 in the L_α system and to -0.85 in the presence of 30 wt % PPI-G2) were recorded. Thus, the major effects of the entrapment of PPI-G2 on the macroscopic rheological properties of the systems are greater elasticity and increased solidlike response. These findings are well correlated with the microscopic picture of the $L_\alpha \rightarrow H_{II}$ transition as reflected by SAXS measurements. Obviously, as already indicated by Fourier transform infrared (FTIR) analysis,¹ during the $L_\alpha \rightarrow H_{II}$ transition PPI was mostly intercalated in the water–lipid interfacial region and much less in the bulk water, due to the low water concentration in the cylinders and high curvature of the hexagonal system. As a consequence, it can be suggested that the enlarged GMO–water interface induced by the strong chaotropic influence of PPI-G2 is responsible for the transformation into more solidlike behavior.

PPI-G2 was solubilized into the binary Q^{224} bicontinuous diamond cubic phase mesophase^{20,22} composed of GMO (65 wt %) and water (35 wt %). While there was no change in the phase symmetry at 5 wt % PPI-G2, a reduction of the lattice parameter by ~ 7.5 Å from ~ 125 to ~ 117.5 Å was detected. When the concentration of PPI-G2 was further increased (10–30 wt %), a $Q^{224} \rightarrow H_{II}$ transition occurred, according to SAXS measurements.¹

A significant decrease of up to ~ 6 Å from ~ 52 to ~ 46 Å in the lattice parameter was measured in the presence of 10–30 wt % PPI-G2 molecule. PPI-G2 entrapment into the Q^{224} mesophase showed a marked and very different effect of PPI-G2 on the rheological properties of the liquid crystalline structures.

As shown in Figure 2a, elastic moduli of the cubic mesophases (without PPI-G2 and at 5 wt % dendrimer) are higher by about 2 orders of magnitude over the viscous moduli in the whole examined frequency range. In addition, while G' is not dependent on the angular frequency, G'' decreased steadily as the frequency increased, indicating the highly elastic three-dimensional structure of the cubic structures.¹⁸ Incorporation of PPI-G2 (5 wt %) decreased the elasticity of the cubic phase and further increased with the PPI-G2 content (starting from 10 wt %), causing a sharp concentration-dependent decline in the values of the elastic moduli and an increase in the loss moduli values. Moreover, greater dependence of the moduli on frequency was clearly observed in the case of the H_{II} mesophases, compared to the empty cubic samples. These findings are a sign of weaker network structure and less distinct

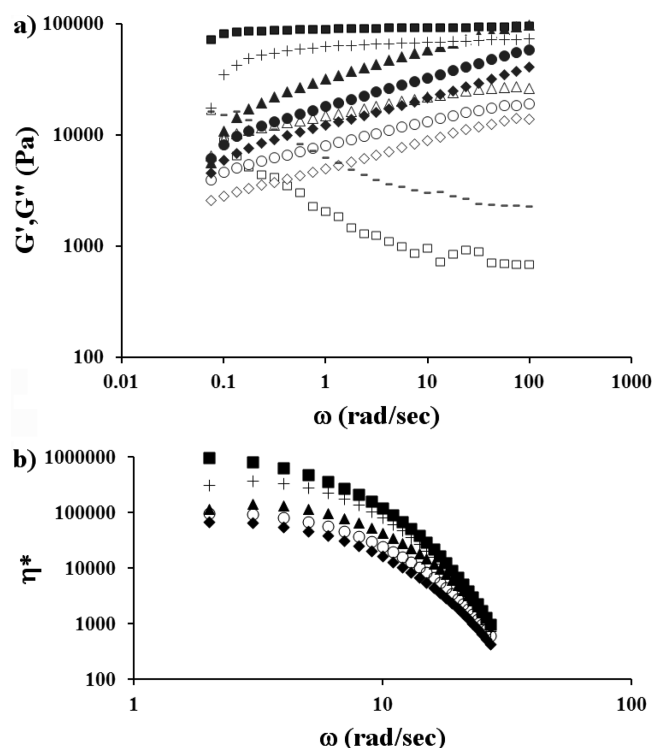


Figure 2. (a) Dynamic frequency sweep test for GMO (65 wt %) and aqueous phase (35 wt %) containing G' (■) and G'' (□), G' (+) and G'' (−), G' (▲) and G'' (△), G' (●) and G'' (○), and G' (◆) and G'' (◇) of 0, 5, 20, 25, and 30 wt % PPI-G2 at 25 °C. (b) Complex viscosity η^* as a function of the applied oscillation frequency (ω) of GMO (65 wt %) and 35 wt % aqueous phase containing (■) 0, (+) 5, (▲) 20, (●) 25, and (◆) 30 wt % PPI-G2, all at 25 °C.

interactions in the mesophases loaded with PPI-G2. Thereby, the $Q^{224} \rightarrow H_{II}$ transition was easily distinguished by the rheological approach. This was confirmed by the frequency dependence of the complex viscosity (Figure 2b), which is significantly higher in cubic phases. The complex viscosity was fitted to a power law (Table 1). Substantial drops in both S and m values were recorded, suggesting more a liquidlike response of the systems loaded with PPI-G2. These results are well correlated with the microscopic picture revealed by SAXS and FTIR analysis. The gradual shrinking of the lattice parameter pointed to a partial dehydration of the hydrophilic headgroups of the glycerol monooleate, probably due to competition for water binding between the PPI-G2 and the polar moieties of the lipid, which caused the $Q^{224} \rightarrow H_{II}$ transition. PPI-G2 was found to act as a “water pump” and competed with the lipid headgroups for water binding. This dehydration process probably decreased the area of monoolein polar moieties and induced both the $Q^{224} \rightarrow H_{II}$ structural shift and the subsequent decrease of the lattice parameter of the H_{II} systems at higher PPI-G2 concentrations.

PPI-G2 was directly incorporated within the hexagonal structures composed of GMO/VE (90/10 ratio)^{21,28,29} and water (20 wt %) at a concentration range of 5–30 wt %. The hexagonal symmetry was retained over all the examined concentration range; however, SAXS measurements demonstrated two trends in the behavior of the lattice parameter. A minor increase in the lattice parameter values (~ 2.5 Å) from 54.5 to 55.3 Å was recorded at low concentrations of PPI-G2 (up to 10 wt %). At higher PPI-G2 content (10–30 wt %), the

lattice parameter values exhibited a notable decrease of ~ 4.5 Å from 56.7 to 52.5 Å. It was inferred that in a low concentration region of PPI-G2 (up to 10 wt %) the dendrimer is probably at least partly intercalated into the interface and interacts with the lipid headgroups.¹ This may expand the interface area and thus slightly increase the lattice parameter. However, the interactions of PPI-G2 with water apparently became dominant upon further PPI-G2 solubilization (greater than 10 wt %), leading to dehydration of the GMO headgroups and a reduction in the lattice parameter, similar to the behavior observed in the L_α and Q^{224} mesophases. These microscopic interactions were further reinforced by the obtained complex viscosity of the H_{II} structures, fitted to the power law (Figure 3a).

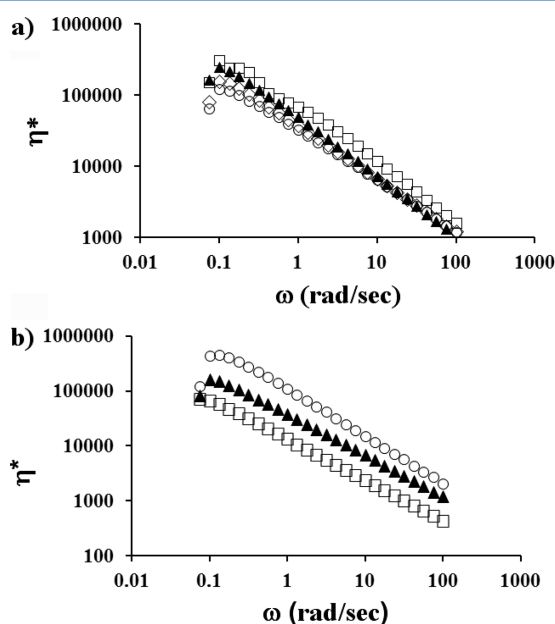


Figure 3. (a) Complex viscosity η^* as a function of the applied oscillation frequency (ω) of GMO/VE 90/10 ratio (72 and 8 wt %) and 20 wt % aqueous phase containing (\square) 0, (\blacktriangle) 10, (\circ) 25, and (\diamond) 30 wt % PPI-G2, all at 25 °C. (b) Complex viscosity η^* as a function of the applied oscillation frequency (ω) of 30 wt % PPI-G2 loaded systems: (\blacktriangle) GMO (85 wt %) and 15 wt % aqueous phase, (\circ) GMO/VE 90/10 ratio (72 and 8 wt %) and 20 wt % aqueous phase, and (\square) GMO (65 wt %) and 35 wt % aqueous phase, all at 25 °C.

The overall effect of PPI-G2 solubilization was weakening of the molecular interactions and a more liquidlike response of the hexagonal systems, demonstrated by a significant drop in both S and m values in the presence of the dendrimer. It is interesting to find that, in the presence of PPI-G2, the sample with 10 wt % dendrimer, possessing the largest lattice parameter, also showed the most elastic properties. Further increase of PPI-G2 content induced formation of weaker structures. This special phenomenon can be explained by the delicate balance between the effect of formation of new bonds between PPI-G2 and GMO within the lipid–water interface and the dehydration effect of monoolein headgroups. While the dehydration of GMO polar moieties decreased the effective headgroup area, formation of a new H-bond between PPI-G2 and GMO caused an increase of the headgroup areas.

PPI-G2 incorporation into L_α , Q^{224} , and H_{II} mesophases induced formation of three types of hexagonal structures

containing the same weight fraction of PPI-G2 in the aqueous phase, but differing in aqueous phase content, dendrimer localization, and lattice parameters. These systems also revealed different rheological responses at the same PPI-G2 weight fraction from the aqueous phase. For example, at 30 wt % PPI, as plotted in Figure 3b, the H_{II} mesophases with the lowest aqueous phase concentration (15 wt %) possessed the highest complex viscosity and solidlike response, compared to the H_{II} structures with aqueous phase of 20 wt % (intermediate complex viscosity and elasticity) and finally with 35 wt % aqueous phase (the weakest response). It should be noted that these results are in contrast to the rheological behavior of empty hexagonal mesophases, which showed enhanced elasticity and higher complex viscosity with increasing aqueous phase concentration.^{18,24,35} In the present case solubilization of the dendrimer dictated the opposite trend. In light of these results, Bohlin's theory³⁷ was implemented in order to obtain additional insight into the differences between the flow responses of these systems.

Bohlin's³⁷ model, which is also reported in the literature as the "weak-gel model",³⁸ was used to assess the flow character and microstructure of the obtained mesophases using rheological data. According to Bohlin's theory, it is presumed that a flowing substance is divided into several flow units that are responsible for the macroscopic flow observed, which is only the consequence of their cooperative rearrangements. These flow units are supposed to be reflected in the microstructure of the material, in the form of molecular aggregates. The main parameter introduced in this theory is the "coordination number", z , which corresponds to the number of flow units interacting with each other to give the cooperative flow response. According to this theory of the "weak-gel" model, the magnitude of complex modulus is expressed by eq 2:

$$G^*(\omega) = \sqrt{G'(\omega)^2 + G''(\omega)^2} = A\omega^{1/2} \quad (2)$$

where A is a constant that can be interpreted as the "interaction strength" between the flow units, revealing the amplitude of cooperative interactions. Bohlin³⁷ demonstrated that the cooperative flow on the hexagonal phase has a 6-fold coordination, identified with the columnar structure of the mesophase. For lamellar mesophase z is equal to 2, while for a cubic structure it could vary between 6 (simple cubic structure), 8 (body-centered structure), and 12 (face-centered structure). This theory has been used to determine the interaction among aggregates and crystalline domains in hexagonal liquid crystals with nonionic surfactants and block copolymers.^{39,40} The values for H_{II} are reported³⁹ as ~ 6.7 .

Experimental values of $|G^*|$ for the mesophases showed a good fit to eq 2 (data not shown). The values of z measured in this study for the hexagonal mesophases ranged between 3.5 and 7 as a function of the aqueous phase content and PPI-G2 concentration (Figure 4). As plotted in Figure 4, the coordination number increases with concentration in the samples containing 15 wt % aqueous phase, starting from 2.5 in the lamellar mesophase to 4.5–7 in H_{II} structures, which are the highest values of the hexagonal structures studied here. It was implied that in the $L_\alpha \rightarrow H_{II}$ transition PPI-G2 was mostly intercalated in the water–lipid interfacial region and much less in the bulk water, due to the low aqueous phase concentration in the samples (15 wt %) and small lattice parameters of 44.13 Å, as also indicated by attenuated total reflectance FTIR

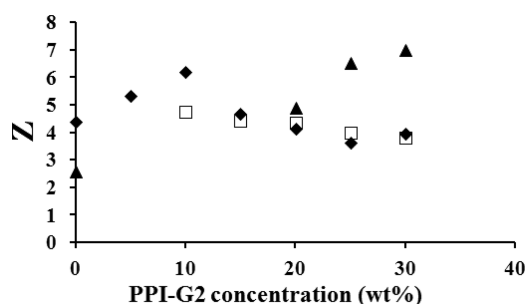


Figure 4. “Coordination number”, z , as a function of PPI-G2 concentration in the three mesophases: (▲) GMO + 15 wt % aqueous phase, (□) GMO + 35 wt % aqueous phase, and (◆) GMO/VE (90/10) + 20 wt % aqueous phase.

measurement. A more tightly packed cylindrical H_{II} structure exhibited a greater number of the flow units interacting with each other due to mechanical forces such as oscillated shearing. During the direct incorporation of PPI-G2 into the hexagonal structures (intermediate water content of 20 wt %), the dendrimer was more equally distributed between the bulk water and the interfacial region. This resulted in higher z numbers at low PPI-G2 content (0–10 wt %) in accordance with the lattice parameter behavior, implying higher PPI-G2 content in the interface. At higher PPI-G2 concentrations (10–30 wt % of PPI) z values dropped to 4, revealing the cooperative response of a smaller number of flow units, due to dehydration of GMO polar heads, accompanied by a decrease in the lattice parameter.¹

In the water-rich cubic samples ($Q^{224} \rightarrow H_{II}$), PPI-G2 was mostly incorporated in the bulk water, resulting in relatively low z numbers that decreased from 4.7 at 10 wt % PPI-G2 content to 3.8 at 30 wt % PPI-G2. Notably, the decrease in z numbers was found to be linear with PPI-G2 concentration, similar to the lattice parameter of the cubic phase (data not shown). It could be inferred that the dehydration of the monoolein polar moieties by PPI-G2 is linearly proportional to both the drop in the lattice parameter and the number of the interacting flow units and the described weaker mechanical properties such as inferior dynamic modulus values and a more liquidlike response upon oscillated perturbation and shearing. Such structural flexibility may be extremely beneficial for controlling and tuning the drug release by dendrimer-inspired mesophase formation possessing the same geometry but different water content, lattice parameters, and rheological properties.

The measured mechanical moduli and complex viscosity of the mesophases were also presented as a function of PPI-G2 concentration at a constant frequency of 0.24 rad/s (Figure 5). This data presentation was employed to comprehend the concentration dependent impact of storage and loss moduli on the complex viscosity. As depicted in Figure 5a, an increase in the complex viscosity in the samples containing 15 wt % aqueous phase can be directly correlated to the measured increase of both G' and G'' . However, a more drastic rise of the elastic modulus, compared to the loss modulus, seemed to be the more dominant contribution to the overall behavior of η^* .

Similar and even more distinct influences of G' on the complex viscosity values were detected in the hexagonal structures with water content of 20 wt % (Figure 5b) and in the water-rich cubic samples at 35 wt % (Figure 5c). In these two cases the trend of the complex viscosity alterations were exactly correlated with the modifications of G' , while the

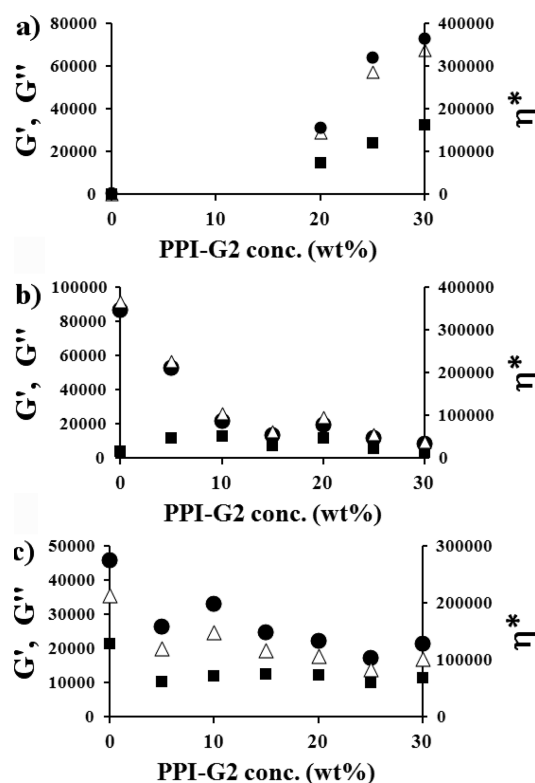


Figure 5. Complex viscosity η^* (Δ), G' (\bullet), and G'' (\blacksquare) as a function of PPI-G2 concentration at $\omega = 0.24$ rad/s of (a) 15 wt % aqueous phase, (b) 35 wt % aqueous phase, and (c) 20 wt % aqueous phase.

influence of G'' was considerably less marked. These findings emphasized that the dendrimer contribution to the mechanical properties of the mesophases is strongly associated with the interfacial elastic properties. Loss moduli were less markedly affected by the PPI presence, and therefore the energy dissipation mechanisms are more related to the inherent host mesophase mechanical behavior rather than to the dendrimer incorporation.

EPR Study. The LLC mesophases depend on physicochemical factors, including surfactant and cosurfactant structure, surfactant and water concentrations, temperature, pH, and solubilize properties and concentration. The EPR study by means of the 5-DSA spin probe provides useful information about microviscosity, micropolarity, and the order of those systems. The probe's amphiphilic characteristic enables its localization between surfactant molecules reporting on the nearby environment of different structures.

The three LLC systems used in this study were investigated using the amphiphilic probe 5-DSA^{30–32} and EPR spectral parameters that were also found to be pH dependent. In this study the pH was 8.6, which is essential for the dendrimer–water solution.

In this basic environment, the probe is ionized (carboxylate anion), and consequently it is pulled toward the water phase due to ion–dipole interactions between the water and the probe, increasing the hydration shell of the latter. This polar structure causes the doxyl group to sense the environment just below the surfactant heads, which are located closer to the aqueous phase.^{31,32}

Empty Mesophases. The EPR spectra for the 5-DSA probe were recorded for the three unloaded mesophases. The EPR spectra of 5-DSA in solution are constituted by the three

hyperfine lines (due to the hyperfine coupling between the unpaired electron spin $S = 1/2$ and the ^{14}N nitrogen nuclear spin $I = 1$) at almost the same intensities. When the probe inserts into a viscous environment, the spectral line shape changes, and the analysis needs the use of a computational procedure that takes into account the relaxation process and the different interactions of the magnetic components. The spectra were computed by means of the well-established procedure of Budil et al.⁴¹ and Schneider and Freed.⁴² To follow the behavior of the system, both the g_{ii} values (measuring the coupling between the electron spin and the magnetic field) and the A_{ii} values (measuring the coupling between the electron spin and the nitrogen nuclear spin) were assumed constant; that is $g_{ii} = 2.009, 2.006$, and 2.003 ; $A_{ii} = 6, 6$, and 33 G ($\langle A \rangle = (1/3)(A_{xx} + A_{yy} + A_{zz}) = 15\text{ G}$), indicating a medium–low polarity environment of the probe. The only parameters that were changed in the fitting procedure were the following: (1) the correlation time for the diffusion rotational motion of the probe, mainly the perpendicular component, τ_{perp} , which reports on the interactions occurring between the nitroxide group and the active sites of the environmental molecules. An increase in τ_{perp} corresponds to an increase in the microviscosity, i.e., a decrease in 5-DSA mobility. The Brownian diffusional model is assumed for which $\tau_{\text{perp}} = 1/(6D_{\text{perp}})$. In this case, as already found in previous studies,^{30–32,43} the computation is not affected by the anisotropy of motion, and therefore, $\tau_{\text{perp}} = \tau_{\text{par}} = \tau$ is assumed. (2) The order parameter, S , which reports on the order of a lipid layer where the probe is embedded. S may change from 0 (no order) to 1 (maximum order). The analysis of the results provides two parameters about the probe's environment: microviscosity and order. The accuracy of the parameters (2–3%) was determined by simulation: variation larger than 3% of a parameter led to a perceptible variation of the simulated line shape, and, consequently, to a worse fit between the simulated and the experimental spectra. Of course other sets of parameters could provide an equivalent or even better fit between the experimental and simulated line shapes, but from several attempted computations, the ones reported are the most confident for the physical meaning of the systems. The experimental and simulated EPR spectra of the unloaded L_{α} , Q^{224} , and H_{II} mesophases in basic medium (pH 8.6) are presented in Figure 6a.

The mobility (τ) and the order parameters (S) obtained from simulation are reported in Table 2. In the L_{α} phase both $\tau = 2.35\text{ ns}$ and $S = 0.356$ indicate a quite fluid but partially ordered environment of the probe that is related to the relatively low viscosity of the L_{α} phase. When the water content increased, i.e., formation of the Q^{224} mesophase, both τ and S increased ($\tau = 3.17\text{ ns}$ and $S = 0.38$), indicating increasing microviscosity and lipid layer order over water concentration. These outcomes are in line with the rheological results, which indicate a “liquidlike structure” for L_{α} and a “solidlike structure” for the Q^{224} mesophases. In the case of the H_{II} mesophase (when VE was added to GMO and water), the EPR spectrum was very noisy, suggesting decreased solubility of the 5-DSA probe into the hexagonal mesophase. Indeed, this spectrum seems to contain a second component in faster and disordered conditions with respect to the first main component. The first peak of the second component is indicated with an arrow in Figure 6a. An attempt to compute the main (ordered) component is shown in Figure 6a by using τ and S equal to 3.56 ns and 0.435 , respectively. The reason for these two

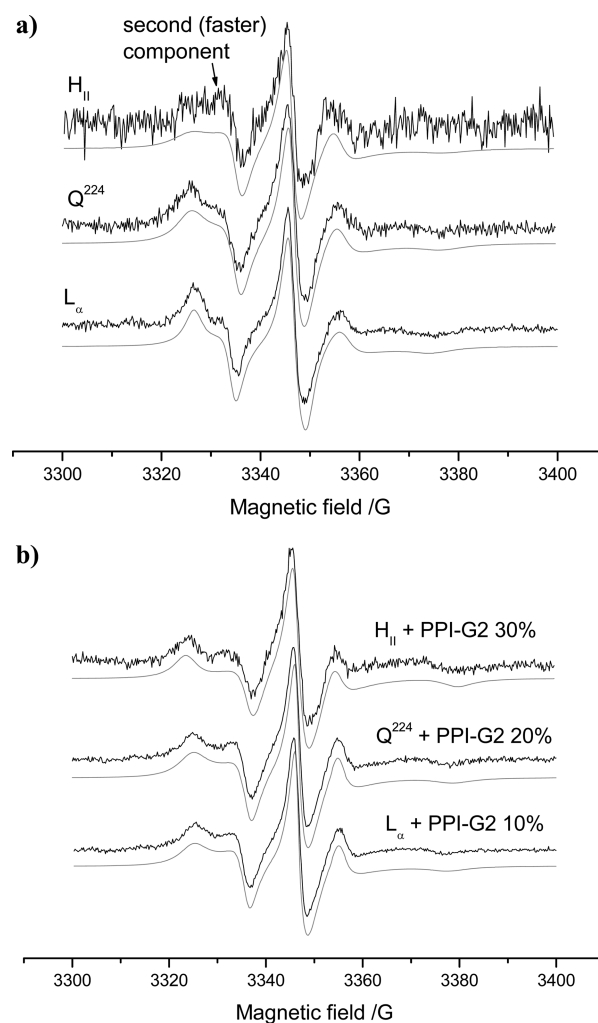


Figure 6. (a) Experimental (black lines) and computed (gray lines) EPR spectra for the three mesophases: L_{α} , GMO + 15 wt % aqueous phase; Q^{224} , GMO + 35 wt % aqueous phase; and H_{II} , GMO/VE (90/10) + 20 wt % aqueous phase. (b) Experimental (black lines) and computed (gray lines) EPR spectra (chosen as examples) for the three mesophases by adding different amounts of PPI-G2: L_{α} (GMO + 15 wt % aqueous phase) + PPI-G2 10%, Q^{224} (GMO + 35 wt % aqueous phase) + PPI-G2 20%, and H_{II} (GMO/VE (90/10) + 20 wt % aqueous phase) + PPI-G2 30%.

environments of the probe, one relatively disordered (S not measurable) and one ordered ($S = 0.435$), is surely due to VE, because in its absence only one component, in a quite ordered condition, was found. It can be assumed that the H_{II} system, which was formed by the addition of the VE molecule, is reorganized in two environments as was observed also by differential scanning calorimetry in previous results from our group.^{21,29} In the disordered environment, VE intercalates and solvates the GMO tails more than in the ordered one. Furthermore, this system is heterogeneous and two components contribute to the spectrum.

PPI-G2 Loaded Mesophases. By solubilizing PPI-G2 within the mesophases, the EPR spectral change is a function of the dendrimer concentration. Figure 6b shows, as examples, the experimental and computed spectra obtained for the L_{α} , Q^{224} , and H_{II} mesophases by adding 10, 20, and 30% PPI-G2, respectively. The microviscosity and order parameters obtained by computation at various dendrimer concentrations are listed

Table 2. Mobility (τ) and Order Parameter (S) Obtained from the Computation of the EPR Spectra of Three Different PPI-G2 Loaded and Unloaded Mesophases at pH 8.6^a

| PPI (wt %) | GMO + 15 wt % aqueous phase | | GMO + 35 wt % aqueous phase | | GMO/VE (90/10) + 20 wt % aqueous phase | |
|------------|-----------------------------|-------|-----------------------------|-------|--|-------|
| | τ (ns) | S | τ (ns) | S | τ (ns) | S |
| 0 | 2.35 | 0.356 | 3.17 | 0.38 | 3.56 | 0.435 |
| 5 | 3.4 | 0.41 | 3.4 | 0.395 | 4.6 | 0.432 |
| 10 | 3.7 | 0.42 | 3.6 | 0.408 | 3.9 | 0.425 |
| 15 | 4.1 | 0.43 | 3.85 | 0.417 | 4.3 | 0.435 |
| 20 | 4.3 | 0.444 | 4.15 | 0.43 | 4.4 | 0.446 |
| 25 | 4.5 | 0.454 | 4.2 | 0.443 | 4.55 | 0.46 |
| 30 | 4.7 | 0.467 | 4.3 | 0.444 | 5.3 | 0.48 |

^aThe three mesophases are GMO + 15 wt % aqueous phase, GMO + 35 wt % aqueous phase, and GMO/VE (90/10) + 20 wt % aqueous phase.

in Table 2. For L_α and Q^{224} both microviscosity and order increase by increasing the PPI-G2 concentration (L_α : from $\tau = 3.4$ ns and $S = 0.41$ at 5 wt % PPI-G2, to $\tau = 4.7$ ns and $S = 0.467$ at 30 wt % PPI-G2; Q^{224} : from $\tau = 3.4$ ns and $S = 0.395$ at 5 wt % PPI-G2, to $\tau = 4.3$ ns and $S = 0.444$ at 30 wt % PPI-G2) (Table 2). If we compare the EPR results for the PPI-G2 loaded systems with the empty L_α and Q^{224} mesophases, we see how PPI-G2 interacts with the water and with the hydroxyl groups of GMO in the interface, perturbing the structure. The main structural changes with increasing PPI-G2 concentration in the L_α and Q^{224} phases are a progressive increase in order and microviscosity. Such results demonstrate how PPI-G2 provokes an order in the interface region and increases the microviscosity by a transformation of the L_α and Q^{224} phases to the H_{II} mesophase. As already seen by SAXS and FTIR,¹ PPI-G2 increased the lattice parameter of the L_α phase by interaction with GMO hydroxyl groups at the interface and increased the CPP. As observed in the Rheological Measurements section, PPI-G2 incorporation increased the elastic properties and pronounced “solidlike” response of the systems. In the case of the Q^{224} mesophase, although the lattice parameter decreases with increasing PPI-G2 concentration, the dendrimer dehydrates the water interface by decreasing the CPP, and the “new” H_{II} mesophase that formed was more ordered since the system reorganized. As a result, the probe mobility decreased and τ increased. It should be mentioned that, at the same PPI-G2 concentration, in Q^{224} the τ and S parameters were the lowest. This is probably due to the strong interaction of PPI-G2 with water, which demonstrated a “liquidlike” behavior in the rheological measurements.

As already found by SAXS and FTIR results, in the H_{II} mesophase two trends can be seen. Up to 10 wt % PPI-G2 τ and S decreased and an increase in those parameters occurred between 15 and 30 wt % PPI-G2. Such results demonstrated the two steps of PPI-G2 solubilization. While PPI-G2 was partly intercalated into the interface and interacted with the lipid headgroups, the interaction with water molecules slightly decreased. As a result, the 5-DSA probe, which inserted closer to the interface, sensed a less ordered system and the rotational mobility of the probe increased. This means that at low PPI-G2 concentration the mobility of the probe within the H_{II} -loaded system was greater than within the empty system. However, when further PPI-G2 was added, PPI-G2 strongly interacted

with water, which caused the dehydration in the interface. Consequently, the system was reorganized in a structure that quenched the probe mobility. At the largest PPI-G2 concentrations the H_{II} mesophase reorganized into a more ordered lipid layer. It should be mentioned that, at 10 wt % PPI-G2, τ and S were the lowest in the H_{II} mesophase. This trend was previously observed by SAXS, FTIR, and rheological measurements as a critical concentration. Thus, it can be concluded that up to this concentration PPI-G2 interacts with the GMO polar hydroxyl groups at the interface. Further solubilization causes the dendrimer to enter the water cylinders.

The influence of an equivalent concentration of PPI-G2 (25 wt %) on the three H_{II} mesophases containing different aqueous phase concentrations and their locations in the three H_{II} phases is illustrated in Figure 7. It can be seen that

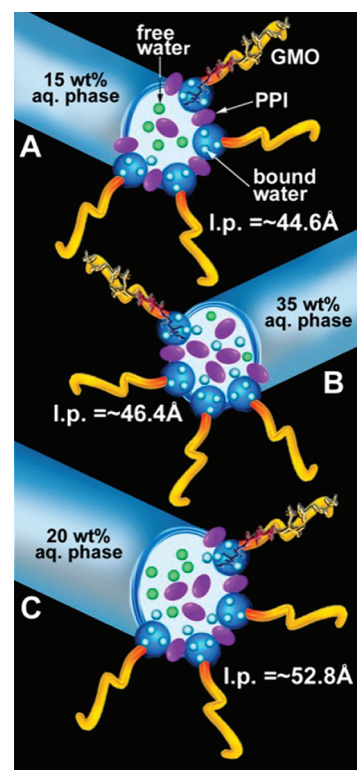


Figure 7. Cartoon illustrating the solubilization location and interactions of PPI-G2 at 25 wt % in different three H_{II} mesophases, containing various aqueous phase concentrations.

introduction of PPI-G2 macromolecules led to their incorporation into the GMO hydroxyl interface (in the case of 15 and 20 wt % aqueous phase) and within the water cylinder (in the case of all mesophases).

CONCLUSIONS

In this study we have explored the macroscopic features of the PPI-loaded L_α , Q^{224} , and H_{II} mesophases as well as the alteration of their molecular level characteristics. The combined data obtained from rheology and EPR spectroscopy, together with the previously published data from the SAXS and FTIR measurements, give a broad and deep insight on the structural effect of the dendrimer.

Incorporation of PPI-G2 into the three lyotropic mesophases induced structural transitions to three types of reverse hexagonal mesophase containing the same weight fraction of

PPI-G2 in the aqueous phase, but differing in aqueous phase concentration, dendrimer solubilization sites, and lattice parameters. These systems also exhibited diverse rheological responses at the same PPI-G2 weight fraction (30 wt %) from the aqueous phase. Notably, while the empty L_α , Q^{224} , and H_{II} systems exhibited typical rheological behavior (an increase in the elasticity with water concentration increase), addition of PPI-G2 into these systems showed the opposite trend.

EPR spectra revealed a gradual increase in the microviscosity and order parameter with increasing PPI-G2 concentration in the L_α mesophases. This increase is in line with the rheological results that indicate a "solidlike" structure for the L_α phase with increasing PPI-G2 concentration. In the case of the Q^{224} mesophase, although the lattice parameter decreases with increasing PPI-G2 concentration, the dendrimer dehydrates the water interface by decreasing the CPP and the "new" H_{II} mesophase that formed was more ordered since the system reorganized. As a result, the probe mobility decreased and τ increased. This system demonstrated a "liquidlike" behavior in the rheological measurements since there was strong interaction of PPI-G2 with water. Two trends were observed in the solubilization of PPI-G2 into the H_{II} mesophase. The addition of PPI-G2 (up to 10 wt %) exhibited a less ordered system with increased rotational mobility, while at further increase the system exhibited a more "solidlike" behavior.

Finally, the following can be concluded: (1) At the L_α phase PPI-G2 interacts with the GMO hydroxyl groups, increasing the CPP, the lattice parameter, the microviscosity, and the order parameter. (2) At the Q^{224} phase the solubilization of the dendrimer caused strong interaction with the water; thus the 5-DSA probe sensed an increase in the microviscosity and order parameter. (3) Two steps of PPI-G2 incorporation took place in the H_{II} mesophase. These steps showed two kinds of interaction: one with the GMO hydroxyl groups at the interface and another with water. The balance with these interactions kept the H_{II} symmetry during PPI-G2 solubilization.

In summary, these results enabled the control of the viscoelastic properties of different H_{II} mesophases by varying the dendrimer concentration, which could be particularly important for practical drug delivery applications.

AUTHOR INFORMATION

Corresponding Author

*Telephone: +972-2-658-6574/5 (N.G.); +972-2-658-4962 (D.L.). Fax: +972-2-652-0262 (N.G.); +972-2-652-0262 (D.L.). E-mail: garti@vms.huji.ac.il (N.G.); dima.libster@mail.huji.ac.il (D.L.).

Notes

The authors declare no competing financial interest.

REFERENCES

- (1) Bitan-Cherbakovsky, L.; Libster, D.; Aserin, A.; Garti, N. *J. Phys. Chem. B* **2011**, *115*, 11984–11992.
- (2) Nir, I.; Aserin, A.; Libster, D.; Garti, N. *J. Phys. Chem. B* **2010**, *114*, 16723–16730.
- (3) Cheng, Y.; Xu, T. *Eur. J. Med. Chem.* **2008**, *43*, 2291–2297.
- (4) Feng, X.; Cheng, Y.; Yang, K.; Zhang, J.; Wu, Q.; Xu, T. *J. Phys. Chem. B* **2010**, *114*, 11017–11026.
- (5) Cheng, Y.; Libo, Z.; Yiwen, L.; Tongwen, X. *Chem. Soc. Rev.* **2011**, *40*, 2673–2703.
- (6) Tomalia, D. A.; Reyna, L. A.; Svenson, S. *Biochem. Soc. Trans.* **2007**, *35*, 61–67.

- (7) Venditto, V. J.; Regino, C. A. S.; Brechbiel, M. W. *Mol. Pharmaceutics* **2005**, *2*, 302–311.
- (8) Caminade, A. M.; Laurent, R.; Majoral, J. P. *Adv. Drug Delivery Rev.* **2005**, *57*, 2130–2146.
- (9) Wolinsky, J. B.; Grinstaff, M. W. *Adv. Drug Delivery Rev.* **2008**, *60*, 1037–1055.
- (10) Cheng, Y.; Wu, Q.; Li, Y.; Hu, J.; Xu, T. *J. Phys. Chem. B* **2009**, *113*, 8339–8346.
- (11) Tomalia, D. A.; Naylor, A. M.; Goddard, W. A. *Angew. Chem., Int. Ed. Engl.* **1990**, *29*, 138–175.
- (12) Jang, W. D.; Selim, K. M. K.; Lee, Ch.H.; Kang, I. K. *Prog. Polym. Sci.* **2009**, *34*, 1–23.
- (13) Nanjwade, B. K.; Bechra, H. M.; Derkar, G. K.; Manv, F. V.; Nanjwade, V. K. *Eur. J. Pharm. Sci.* **2009**, *38*, 185–196.
- (14) Klajnert, B.; Cortijo-Arellano, M.; Bryszewska, M.; Cladera, J. *Biochem. Biophys. Res. Commun.* **2006**, *339*, 577–582.
- (15) Ottaviani, M. F.; Mazzeo, R.; Cangiotti, M.; Fiorani, L.; Majoral, J. P.; Caminade, A. M.; Pedziwiatr, E.; Bryszewska, M.; Klajnert, B. *Biomacromolecules* **2010**, *11*, 3014–3021.
- (16) Witvrouw, M.; Fikkert, V.; Pluymers, W.; Matthews, B.; Mardel, K.; Schols, D.; Raff, J.; Debyser, Z.; De Clercq, E.; Holan, G.; Pannecouque, C. *Mol. Pharmacol.* **2000**, *58*, 1100–1108.
- (17) Gajbhiye, V.; Palanirajan, V. K.; Tekade, R. K.; Jain, N. K. *J. Pharm. Pharmacol.* **2009**, *61*, 989–1003.
- (18) Mezzenga, R.; Meyer, C.; Servais, C.; Romoscanu, A. I.; Sagalowicz, L.; Hayward, R. C. *Langmuir* **2005**, *21*, 3322–3333.
- (19) Libster, D.; Ben Ishai, P.; Aserin, A.; Shoham, G.; Garti, N. *Langmuir* **2008**, *24*, 2118–2127.
- (20) Amar-Yuli, I.; Garti, N. *Colloids Surf., B* **2005**, *43*, 72–82.
- (21) Bitan-Cherbakovsky, L.; Yuli-Amar, I.; Aserin, A.; Garti, N. *Langmuir* **2009**, *25*, 13106–13113.
- (22) Hyde, S. T. In *Handbook of Applied Surface and Colloid Chemistry*; Holmberg, K., Ed.; Wiley: New York, 2001; Chapter 16, pp 299–332.
- (23) Drummond, C. J.; Fong, C. *Curr. Opin. Colloid Interface Sci.* **2000**, *4*, 449–456.
- (24) Libster, D.; Aserin, A.; Wachtel, E.; Shoham, G.; Garti, N. *J. Colloid Interface Sci.* **2007**, *308*, 514–524.
- (25) Libster, D.; Aserin, A.; Yariv, D.; Shoham, G.; Garti, N. *J. Phys. Chem. B* **2009**, *113*, 6336–6346.
- (26) Mishraki, T.; Libster, D.; Aserin, A.; Garti, N. *Colloids Surf., B* **2010**, *75*, 47–56.
- (27) Cohen-Avrahami, M.; Aserin, A.; Garti, N. *Colloids Surf., B* **2010**, *77*, 131–138.
- (28) Bitan-Cherbakovsky, L.; Yuli-Amar, I.; Aserin, A.; Garti, N. *Langmuir* **2010**, *26*, 3648–3653.
- (29) Amar-Yuli, I.; Aserin, A.; Garti, N. *J. Phys. Chem. B* **2008**, *112*, 10171–10180.
- (30) Mishraki, T.; Ottaviani, M. F.; Shames, A. I.; Aserin, A.; Garti, N. *J. Phys. Chem. B* **2011**, *115*, 8054–8062.
- (31) Kogan, A.; Rozner, S.; Mehta, S.; Somasundaran, P.; Aserin, A.; Garti, N.; Ottaviani, M. F. *J. Phys. Chem. B* **2009**, *113*, 691–699.
- (32) Rozner, S.; Kogan, A.; Mehta, S.; Somasundaran, P.; Aserin, A.; Garti, N.; Ottaviani, M. F. *J. Phys. Chem. B* **2009**, *113*, 700–707.
- (33) Montalvo, G.; Valiente, M.; Rodenas, E. *Langmuir* **1996**, *12*, 5202–5208.
- (34) Cordobés, F.; Muñoz, J.; Gallegos, C. J. *Colloid Interface Sci.* **1997**, *187*, 401–417.
- (35) Amar-Yuli, I.; Wachtel, E.; Shalev, D. E.; Aserin, A.; Garti, N. *J. Phys. Chem. B* **2008**, *112*, 3971–3982.
- (36) Achrai, B.; Libster, D.; Aserin, A.; Garti, N. *J. Phys. Chem. B* **2011**, *115*, 825–835.
- (37) Bohlin, L. *J. Colloid Interface Sci.* **1980**, *74*, 423–434.
- (38) Gabriele, D.; De Cindio, B.; D'Antona, P. *Rheol. Acta* **2001**, *40*, 120–127.
- (39) Rodríguez-Abreu, C.; Aramaki, K.; Kunieda, H. *Colloids Surf., A* **2005**, *269*, 59–66.

- (40) Alam, M. M. Formation and rheological behavior of hexagonal and cubic phase based gel emulsions. Ph.D. Dissertation, Yokohama National University, September 2009.
- (41) Budil, D. E.; Lee, S.; Saxena, S.; Freed, J. H. *J. Magn. Reson., Ser. A* **1996**, *120*, 155–189.
- (42) Schneider, D. J.; Freed, J. H. Slow Motional Magnetic Resonance Spectra: A User's Guide. In *Biological Magnetic Resonance*; Berliner, L. J., Reuben, J., Eds.; Plenum Press: New York, 1989; Vol. 8, pp 1–76.
- (43) Galarneau, A.; Sartori, F.; Cangiotti, M.; Mineva, T.; Di Renzo, F.; Ottaviani, M. F. *J. Phys. Chem. B* **2010**, *114*, 2140–2152.